A Zeno-Free Event-Triggered Secondary Control for AC Microgrids

Abdolmaleki, Babak; Shafiee, Qobad; Seifi, Ali Reza; Arefi, Mohammad Mehdi; Blaabjerg, Frede

Published in:
IEEE Transactions on Smart Grid

DOI (link to publication from Publisher):
10.1109/TSG.2019.2945250

Publication date:
2020

Document Version
Accepted author manuscript, peer reviewed version

A Zeno-Free Event-Triggered Secondary Control for AC Microgrids

Babak Abdolmaleki, Qobad Shafiee, *Senior Member, IEEE,* Ali Reza Seifi, Mohammad Mehdi Arefi, *Senior Member, IEEE,* and Frede Blaabjerg, *Fellow, IEEE*

***Abstract*—This paper proposes a secondary voltage, frequency, and active power sharing control for autonomous inverter-based microgrids with event-triggered communications. A proportional-integral consensus-based control scheme is introduced which benefits from need-based (event-triggered) data exchange among distributed generators. The employed event-triggering condition *i*) ensures the system stability, *ii*) ensures that the system is Zeno-free and there exists a controllable minimal inter-event time, *iii*) removes the redundant communications during both transient and steady-state stages, *iv*) accounts for directed communication network architectures, and *v*) is fully distributed from both design and implementation standpoints. Effectiveness of the proposed controller for various case studies is verified via MATLAB/Simulink-based simulations. Comparison between different cases and conventional strategies are also included.**

***Index Terms*—Consensus algorithm, event-triggered control, frequency control, microgrid, power sharing, secondary control, voltage control, Zeno behavior.**

NOMENCLATURE

δ_i	i^{th} distributed generator's (DG's) phase angle.
P_i, Q_i	i^{th} DG's measured active & reactive powers.
$\hat{P}_i, \hat{Q}_i$	i^{th} DG's actual active & reactive powers.
P_i^*, Q_i^*	i^{th} DG's rated active & reactive powers.
f_i, V_i	i^{th} DG's output frequency & voltage.
f^*, V^*	Rated frequency & voltage.
f_{ref}, V_{ref}	Reference frequency & voltage.
f_c	Power measurement filter's cutoff frequency.
m_i, n_i	Droop coefficients.
Ω_i, Γ_i	Frequency & voltage correction terms.
G_{ij}, B_{ij}	Conductance & susceptance among DGs i & j.
G_{ii}, B_{ii}	i^{th} DG's shunt conductance & susceptance.
$\overline{\Delta f}, \overline{\Delta V}$	Maximum frequency & voltage deviations.
K_i^f, K_i^V	Nonnegative proportional gains.
I_i^f, I_i^V	Nonnegative integral gains.
b_i^f, b_i^V, b_i^Ω	Logical indicators.
a_{ij}	Communication weighting from j^{th} DG to i^{th} DG.
d_i, d_i^o	i^{th} DG's in-degree & out-degree in the CN.
$\mathcal{A}, \mathcal{D}, \mathcal{L}$	CN's matrices. Refer to Section II-A.
$t_{k_i}^i$	k_i^{th} triggering instant associated with i^{th} DG.
t_i, t_0^i	i^{th} DG's local clock and activation instant.
$\tilde{\Omega}_i, \tilde{V}_i$	The latest sampled signals of Ω_i, V_i at $t_{k_i}^i$.
τ	Minimal inter-event (inter-communication) time.
σ	Positive parameter governing the state-dependent part of the triggering conditions in (8).
γ_Ω, γ_V	Positive parameters governing the constant parts of the triggering conditions in (8).
$\mathbf{1}_n, \mathbf{0}_n$	Vectors of ones and zeros in $\mathbb{R}^n$.
$\mathcal{I}_n$	Identity matrix in $\mathbb{R}^{n\times n}$.

Manuscript received September 10, 2018; revised March 25, 2019, July 28, 2019; accepted September 22, 2019. Date of publication XXXX XX, XXXX; date of current version XXXX XX, XXXX. Paper no. TSG-01323-2018.

B. Abdolmaleki and Q. Shafiee are with the Smart/Micro Grids Research Center (SMGRC), University of Kurdistan, Sanandaj, Iran (e-mail: abdolmaleki.p.e@gmail.com, q.shafiee@uok.ac.ir).

A. R. Seifi and M. M. Arefi are with the School of Electrical and Computer Engineering, Shiraz University, Shiraz, Iran (e-mail: seifi@shirazu.ac.ir, arefi@shirazu.ac.ir).

F. Blaabjerg is with the Department of Energy Technology, Aalborg University, Denmark (e-mail: fbl@et.aau.dk).

Color versions of one or more of the figures in this paper are available online at http://ieeexplore.ieee.org.

Digital Object Identifier XX.XXXX/TSG.20XX.XXXXXXX

I. INTRODUCTION

SECONDARY CONTROL of islanded microgrids (MGs) compensates for voltage and frequency deviations caused by droop control as well as provides proper power sharing between distributed generators (DGs) [1]. This control level is realized by using a communication network (CN). Therefore, distributed control architectures using sparse CNs, are preferred to the centralzied ones with complex CNs [2].

Most of the previous works in the context of secondary control are conducted based on the continuous CNs (e.g. see [3]–[14]), while the realistic data exchange infrastructures are sample-based and have limited bandwidths [15], [16]. Thus, from a system scaling standpoint, efficient usage of communication medium is mandatory. In networked control systems, a solution to avoid probable network congestions and reduce the communication burden is to use event-triggered (ET) control strategies eliminating redundant communications [17], [18]. Generally, ET control is a strategy under which the desired state is sampled and broadcasted, and the control rule is updated (i.e., an event is triggered), only if some condition(s) is(are) satisfied. Any ET condition must satisfy two system requirements: Stability and Zeno-freeness. *Zeno behavior* is a phenomenon under which excessive redundant events are triggered over a finite time interval. Because of limited communication and computational capabilities, no control system can be implemented on a digital platform, if the behavior exists [17], [18].

Triggered control of MGs has been introduced in the literature [19]–[28]. Reference [19], proposes a self-triggered coordinated power control scheme for ac MGs where the next event time is determined at any current event time. Thus, the controller cannot respond quickly to the disturbances. A distributed ET load sharing control is proposed in [20]. In this work, an average-consensus algorithm is used to control the inter-DG active power

sharing by controlling their output currents. A distributed ET reactive power sharing control is proposed in [21]. Similarly, a current sharing controller for dc MGs is proposed in [22]. In both of these works, consensus algorithms with nonlinear state feedback are presented, providing proper reactive power sharing and proper current sharing respectively. To address the voltage regulation in converter-based dc MGs, the work in [22] is extended in [23]. In [24], an event-based consensus control is introduced to achieve proper active power sharing among a cluster of ac and dc MGs. In this work, each interlinking converter is considered as an agent which utilizes this event-based controller to share the active powers properly between the MGs. ET secondary control of dc MGs is investigated in [25]. In this work, a full-state feedback ET controller is designed which also uses full-state observation to detect the event times. None of the above works accounts for ET secondary voltage and frequency control of MGs. These problems have been addressed in [26]–[28]. A distributed ET secondary voltage and frequency control is proposed in [26]. The proposed ET conditions in this work, however, do not reduce the communication burden significantly and even may result in Zeno behavior, though the theoretical Zeno exclusion analysis is provided (see [17, Sec. III-A] for more info). In [27], [28], some secondary controllers with ET communications are proposed where the working frequency of the digital communication platform (infrastructure) is not considered. In fact, therein it is assumed that the inter-event time intervals can get any positive value and there is no specific lower bound restriction on the intervals. Moreover, the work in [26], similar to [3]–[11], is based on leader-following consensus algorithm [29] of frequency, i.e., the frequency is treated as a communication data. However, in power systems, frequency is a global entity and hence a frequency-consensus control seems to be redundant. Furthermore, the secondary compensation terms are usually generated by using a pure integrator which leads to a poor transient response, e.g., see [3]–[11], [26]–[28].

Motivated by the above statements and literature, this paper deals with event-triggering of communications, in secondary voltage and frequency control of MGs. Salient features of the proposed control scheme are as follows.

C1: A *proportional-integral-based* (PI-based) secondary control is proposed based on consensus algorithm. Unlike [19]–[25], [27], the voltage, frequency, and active power sharing control tasks are considered simultaneously. Moreover, different from [3]–[11], [26] the only communication data in frequency-power control are frequency correction terms.

C2: A triggering condition is proposed which *i*) ensures that the system is Zeno-free with inter-event time intervals greater than a *desired time constant*, *ii*) is fully distributed from both design and implementation standpoints providing scalablity and plug-and-play capability, *iii*) benefits from a constant threshold, reducing the communications more effectively, especially in steady state, and *iv*) accounts for directed CNs.

C3: A systematic stability analysis with ultimate uniform boundedness approach is provided. The impacts of design parameters on system's performance and communication pattern are studied as well. Moreover, the results are compared with those under some other existing strategies.

The rest of this paper is structured as follows. Section II provides the MG's modeling. The proposed controller is designed in Section III. Simulation results for different cases are included in Section IV. Finally, Section V concludes the paper.

II. System Modeling

A. Communication Network (CN) Layer

The CN of a MG can be regarded as a directed graph with the DGs and the communication links playing the roles of its nodes and edges, respectively. Consider the graph $\mathcal{G} \subseteq (\mathcal{N}, \mathcal{E}, \mathcal{A})$, where, $\mathcal{N} = \{1, ..., n\}$, $\mathcal{E} \subseteq \mathcal{N} \times \mathcal{N}$, and $\mathcal{A} = [a_{ij}] \in \mathbb{R}^{n\times n}$ are its node set, edge set, and adjacency matrix, respectively. If node i obtains data from node j, then node j is an in-neighbor of node i, node i is an out-neighbor of node j, $(j,i) \in \mathcal{E}$, and $a_{ij} = 1$; otherwise, nodes j and i are not neighbors, $(j,i) \notin \mathcal{E}$, and $a_{ij} = 0$. Let $N_i = \{j \mid (j,i) \in \mathcal{E}\}$, $N_i^o = \{j \mid (i,j) \in \mathcal{E}\}$, $d_i = \sum_{j\in N_i} a_{ij}$, and $d_i^o = \sum_{j\in N_i^o} a_{ji}$ be the in-neighbor set, out-neighbor set, in-degree, and out-degree of node i, respectively. Laplacian matrix of $\mathcal{G}$ is $\mathcal{L} = \mathcal{D} - \mathcal{A}$, where, $\mathcal{D} = diag\{d_i\}$ (proper diagonal matrix). A path from node j to node i is a sequence of pairs, belong to $\mathcal{E}$, expressed as $\{(j, n_1), ..., (n_m, i)\}$. A graph has a spanning tree, if there exists a node (called root node) from which there exists a path to any other node within the graph [29], [30].

B. Physical and Control Layers

From Fig. 1, each DG comprises a voltage sourced inverter, a LC filter, inner current and voltage controllers, power measurement filters, and a droop-control unit. Details on the design of these parts are provided in [31], [32]. The inner controllers are normally designed such that the subsystem comprising them, the inverter, and LC filter has a high bandwidth but the average power measurement filters are very slow. Therefore, neglecting the dynamics of the mentioned subsystem, one can consider each DG as a droop-controlled voltage source which is connected to the rest of the MG through a connector. The state model of i^{th} DG can then be expressed as [33]

$$\dot{\delta}_i = 2\pi f_i, \tag{1a}$$
$$\dot{P}_i = 2\pi f_c(\hat{P}_i - P_i), \tag{1b}$$
$$\dot{Q}_i = 2\pi f_c(\hat{Q}_i - Q_i), \tag{1c}$$
$$f_i = f_{nom} + \Omega_i - m_i P_i, \tag{1d}$$
$$V_i = V_{nom} + \Gamma_i - n_i Q_i. \tag{1e}$$

In a Kron-reduced electric network model [33], $\hat{P}_i$ & $\hat{Q}_i$ are as

$$\hat{P}_i = G_i V_i^2 + \sum\nolimits_j V_i V_j G_{ij} \cos(\delta_i - \delta_j) + \sum\nolimits_j V_i V_j B_{ij} \sin(\delta_i - \delta_j), \tag{2a}$$
$$\hat{Q}_i = -B_i V_i^2 - \sum\nolimits_j V_i V_j B_{ij} \cos(\delta_i - \delta_j) + \sum\nolimits_j V_i V_j G_{ij} \sin(\delta_i - \delta_j), \tag{2b}$$

where, $G_i = G_{ii} + \sum_j G_{ij}$, $B_i = B_{ii} + \sum_j B_{ij}$.

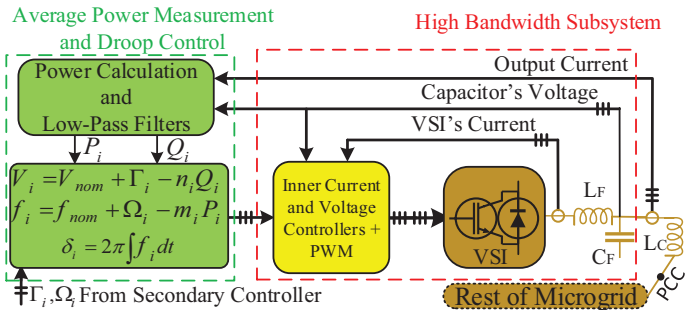

Fig. 1. Physical and control layers of i^{th} distributed generation unit (DG).

III. Secondary Control Design

The aim is to shift the droop characteristics along the voltage and frequency axes, so that in steady state one has

$$[V_i, f_i, m_i P_i]^T \to [V_{ref}, f_{ref}, m_j P_j]^T, \quad \forall i, j. \tag{3}$$

This aim ensures proportional active power sharing between the DGs, if one selects $m_i = \overline{\Delta f}/P_i^*$ and $n_i = \overline{\Delta V}/Q_i^*$ [32].

Remark 1: Because of line impedance effect, accurate voltage regulation leads to poor reactive power sharing and vice versa [13]. Therefore, following the research line composed of the works in [3]–[11], [26], this paper focuses on the voltage regulation task, and reactive power responses are omitted for brevity. In addition, the ET reactive power controller provided in [21] can be modified slightly, to cover the directed CNs.

A. Event-Triggered PI-based Secondary Control

Once the DGs talk to each other via the CN described in Section II-A, the aim in (3) can be achieved by using a consensus-based secondary control [4]–[11], [29]. In this way, the following proportional-integral-based (PI-based) correction terms are proposed for i^{th} DG.

$$\Omega_i = K_i^f (b_i^f \Delta f_i + b_i^\Omega \tilde{z}_i^\Omega) + I_i^f \int (b_i^f \Delta f_i + b_i^\Omega \tilde{z}_i^\Omega) dt, \tag{4a}$$

$$\Gamma_i = n_i \int \dot{Q}_i dt + K_i^V \left(b_i^V \Delta V_i + (1 - b_i^V)\tilde{z}_i^V\right) + I_i^V \int \left(b_i^V \Delta V_i + (1 - b_i^V)\tilde{z}_i^V\right) dt, \tag{4b}$$

$$\Delta f_i = f_{ref} - f_i, \;\; \tilde{z}_i^\Omega = \left(\tfrac{1}{d_i}\sum\nolimits_j a_{ij}\tilde{\Omega}_j\right) - \tilde{\Omega}_i, \tag{5a}$$

$$\Delta V_i = V_{ref} - V_i, \;\; \tilde{z}_i^V = \left(\tfrac{1}{d_i}\sum\nolimits_j a_{ij}\tilde{V}_j\right) - \tilde{V}_i, \tag{5b}$$

where, if the DG has direct access to f_{ref} (resp. V_{ref}), then $b_i^f = 1$ (resp. $b_i^V = 1$), otherwise $b_i^f = 0$ (resp. $b_i^V = 0$); if the DG cooperates with its in-neighbors $b_i^\Omega = 1$, otherwise $b_i^\Omega = 0$. The *local parts* in (4) employ the continuous local signals f_i, V_i, and $\dot{Q}_i$, while the *neighborhood errors* $\tilde{z}_i^f, \tilde{z}_i^V$ use the latest sampled communication data as follows.

$$\begin{cases} \tilde{\Omega}_i(t) = \Omega_i(t_{k_i}^i), \\ \tilde{V}_i(t) = V_i(t_{k_i}^i), \end{cases} \quad t \in [t_{k_i}^i, t_{k_i+1}^i), \; k_i = 0, 1, \cdots. \tag{6}$$

The triggering instant $t_{k_i}^i$ is when the signals V_i and Ω_i are sampled and transmitted to the out-neighbors. Please, note that over $[t_{k_i}^i, t_{k_i+1}^i)$ the signals $\tilde{\Omega}_i$ and $\tilde{V}_i$ remain constant, while the neighbors' latest received data, i.e., $\tilde{\Omega}_j$ and $\tilde{V}_j, \forall j$ may vary.

Remark 2: The data exchange among the DGs is normally realized by using a wireless/wired CN with time-triggered signal transmission strategy. In this strategy, a high frequency periodic data sampling and communication should be adopted to implement the controller in (4) such that the time interval between any two consecutive triggering instants are equal to a sampling time τ_s, i.e., $t_{k_i+1}^i - t_{k_i}^i = \tau_s, \forall i, k$.

Although the periodic transmission strategy provides a good performance, it leads to many redundant data exchanges, especially in steady state, when the control goal is achieved and not so many communications are required. Thus, an ET control under which every DG decides on its own to sample and transmit data to CN *only when it is needed* seems effective.

Question: Now, the question is that, when are the right triggering instants $t_{k_i}^i$, $k_i = 0, 1, \cdots$–the instants when, each DG decides on its own to sample its local data Ω_i and V_i, and to broadcast these samples–?

Answer: The appropriate triggering instants should be designed such that, *i*) performance of the system undergoes a little degradation while using $\tilde{\Omega}_i$ & $\tilde{V}_i$ instead of Ω_i & V_i in (5), and *ii*) the intervals between consecutive triggering instants have a lower bound τ which is the digital communication platform's (infrastructure's) capability (working frequency).

One way is to control the deviations of the continuous signals Ω_i, V_i from their latest sampled quantities $\tilde{\Omega}_i, \tilde{V}_i$, i.e., $e_i^\Omega = \tilde{\Omega}_i - \Omega_i$ and $e_i^V = \tilde{V}_i - V_i$. To this end, one should compare $|e_i^\Omega|$ and $|e_i^V|$ with some thresholds, every τ seconds. The employed thresholds should comprise a state-dependent part and a constant part [17]. The state-dependent part governs the triggering pattern over transients and usually converges to zero in steady state. Hence, to avoid trigger chattering in steady state, the constant part is included [17]. Accordingly, the following triggering instant is proposed for i^{th} DG.

$$t_{k_i+1}^i = \inf\{t_i > t_{k_i}^i + \tau : \text{(8a) or (8b)}\}, \tag{7}$$

$$\text{where,} \quad |e_i^\Omega| > \sigma b_i^\Omega |\tilde{z}_i^\Omega| + \gamma_\Omega, \tag{8a}$$

$$|e_i^V| > \sigma (1 - b_i^V) |\tilde{z}_i^V| + \gamma_V, \tag{8b}$$

where, $\tilde{z}_i^\Omega = \frac{1}{d_i}\sum a_{ij}(\tilde{\Omega}_j - \tilde{\Omega}_i)$, $\tilde{z}_i^V = \frac{1}{d_i}\sum a_{ij}(\tilde{V}_j - \tilde{V}_i)$ are the local neighborhood errors; inf denotes the infimum sign. The proposed ET controller is explained in Algorithm 1.

Remark 3: In (7), the triggering conditions in (8) are checked every τ seconds (not continuously); therefore, in addition to the communication burden, the computational burden is accordingly reduced. Moreover, if τ be selected greater than or equal to the communication medium's working sampling time, one can ensure that Zeno phenomenon (sampling chattering) is canceled out. Note that b_i^Ω and b_i^V indicate whether i^{th} DG cooperates with its in-neighbors or not. Therefore, they are included to make (8a) and (8b) adaptive to this issue.

B. Design Guidelines and Requirements

In what follows, based on the upcoming theoretical analyses in Appendix A, the readers are provided with some design hints.

Algorithm 1 The proposed event-triggering algorithm.

initialization: ▷ The first triggering instant
Sample $\tilde{\Omega}_i \leftarrow \Omega_i$, $\tilde{V}_i \leftarrow V_i$, and $\tilde{t}_i \leftarrow t_i$
Store the samples in the Data Store Unit (DSU)
Send $\tilde{\Omega}_i$ and $\tilde{V}_i$ to out-neighbors
Compute Ω_i and Γ_i in (4a) and (4b)
while secondary control is active **do**
  Compute $e_i^{\Omega} = \tilde{\Omega}_i - \Omega_i$, $e_i^{V} = \tilde{V}_i - V_i$, and $t_i - \tilde{t}_i$
  Alert the data receiver
  if $\{t_i - \tilde{t}_i > \tau\}$&{(8a) or (8b) holds} **then** ▷ Trigger
    Do lines 1 to 3 of the algorithm
  end if
  for all $j \in N_i$ **do**
    if new data received **then** ▷ Data receive
      Update and store $\tilde{\Omega}_i$ and $\tilde{V}_i$
    end if
  end for
  Compute Ω_i and Γ_i in (4a) and (4b)
end while

** *t_i (resp. $\tilde{t}_i$) is local clock (resp. latest triggering instant) of i^{th} DG.*

Stability: For stable operation, *i*) the matrix $\mathbf{A}$ in (11) must be Hurwitz; *ii*) each DG must have more in-neighbors than out-neighbors, i.e., $d_i > d_i^o, \forall i$ (cf. Section II-A); *iii*) $\sigma < 0.5$, and $\tau < \min(\tau_0^{\Omega}, \tau_0^{V})$ (cf. (22)).

Desired equilibrium: To achieve the aim in (3) the inter-DG CN must has a spanning tree rooted at a DG with $b_i^f, b_i^V \neq 0$.

Control gains: One should choose the non-negative gains such that the stability requirements are satisfied.

Event-triggering parameters: The triggering conditions contain the 4 parameters τ, γ_Ω, γ_V, and σ_Ω. According to (22), τ can get a wide range of values for stable operation of system. However, the stability may not be enough solely; hence, one should choose τ according to the first part of Appendix A-E. From (26) and (27) one can see that γ_Ω and γ_V determine steady-state frequency and voltage errors, respectively. Therefore, considering $2\gamma_\Omega$ and $2\gamma_V$ as the maximum neighborhood errors one should choose proper gammas. Finally, looking at second part of Appendix A-E one should select σ as large as possible, for instance $\sigma = 0.49$.

IV. Case Studies

To verify the effectiveness of the proposed controller, an islanded 220-V, 50-Hz three-phase 5-bus MG with four DGs is simulated in MATLAB/Simulink environment. Each DG has the dynamics in (1) which feeds its local bus through the connector Z_C. Each feeder line is modeled with a lumped series RL impedance Z_L. The loads are modeled by constant impedance loads. Single-line diagram of the test MG is depicted in Fig. 2 where the electrical and control requirements of different parts are also given. Note that $\overline{\Delta f} = 0.25$-Hz and $\overline{\Delta V} = 11$-V.

A. Performance Assessment: Activation and Load Changes

In this case, the directed CN depicted in Fig. 2, is used for inter-DG communications. The parameters in (8)-(12) are as follows: $\tau^{-1} = 25$-Hz, $K_i^V = K_i^f = 5$, $I_i^V = I_i^f = 10$,

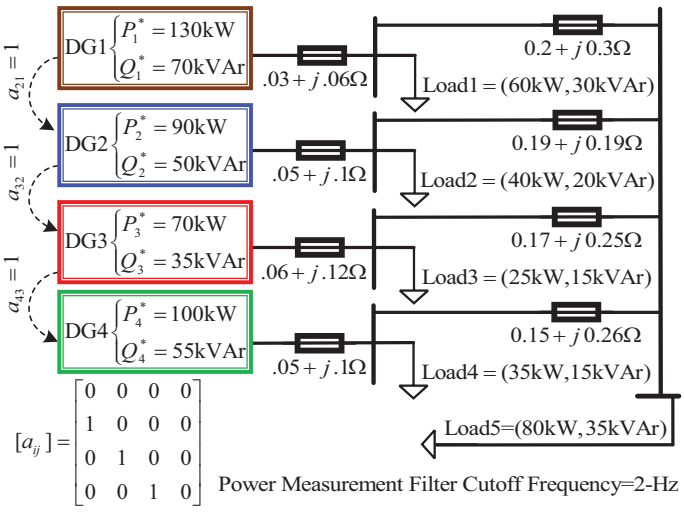

Fig. 2. Test microgrid system; specifications of different parts are also given.

$\mathbf{b}_f = \mathbf{b}_V = [1,0,0,0]^T$, $\mathbf{b}_\Omega = [0,1,1,1]^T$, $\sigma = 0.49$, $\gamma_\Omega = 0.001/2$, and $\gamma_V = 0.05/2$. Fig. 3 indicates the performance of the controller over different stages. Prior to the proposed controller's activation at $t = 4s$, the MG is controlled by droop control. At $t = 8s$, load 5 increases by 33% of total load. Load 5 decreases to its initial value, at $t = 12s$. Fig. 3(a)-(c) indicate that for $t < 3s$ the DGs' voltages and frequencies are deviated from the nominal values, and the active powers are shared properly. Activation of the secondary controller at $t = 4s$ restores the voltages and frequencies to the reference values of 220-V and 50-Hz while guarantees proportional active power sharing between the DGs. It is shown that after load changes at $t = 8s$ and $t = 12s$, the voltages and frequencies are restored back to the reference values, and proportional active power sharing still remains. Fig. 3(d) depicts the triggering (communication) instants for all the DGs. It is indicated that *i*) the communication burden is highly reduced, *ii* most of the communications are triggered during the transient stages, and *iii*) the inter-event time intervals are always greater than τ, i.e., Zeno behavior does not appear.

B. Impacts of Communication Delay and Feedback Gains

Fig. 4 shows the controller performance for the case in Section IV-A, but with $K_i^V = K_i^f = 10$, $I_i^V = I_i^f = 20$ and communication delays of 0 and 160 milliseconds. Comparing Fig. 3(a)-(c) and Fig. 4(a)-(c), it is obvious that, the more feedback gain, the more synchronization speed, and the better transient response. Comparing Fig. 4(a)-(c) and Fig. 4(d)-(f), one can see that the communication delay slows down the synchronization speed and results in some transient oscillations. However, the desired control aim can be reached properly, for a practical range of delays (in the order of tens of milliseconds).

C. Plug-and-Play Capability and Link Failure Investigation

In this case, all the parameters defined in the preamble of Section IV-A are employed again. To preserve connectivity of the CN in Fig. 2, a link is established from DG 1 to DG 4.

This article has been accepted for publication in a future issue of this journal, but has not been fully edited. Content may change prior to final publication. Citation information: DOI 10.1109/TSG.2019.2945250, IEEE Transactions on Smart Grid

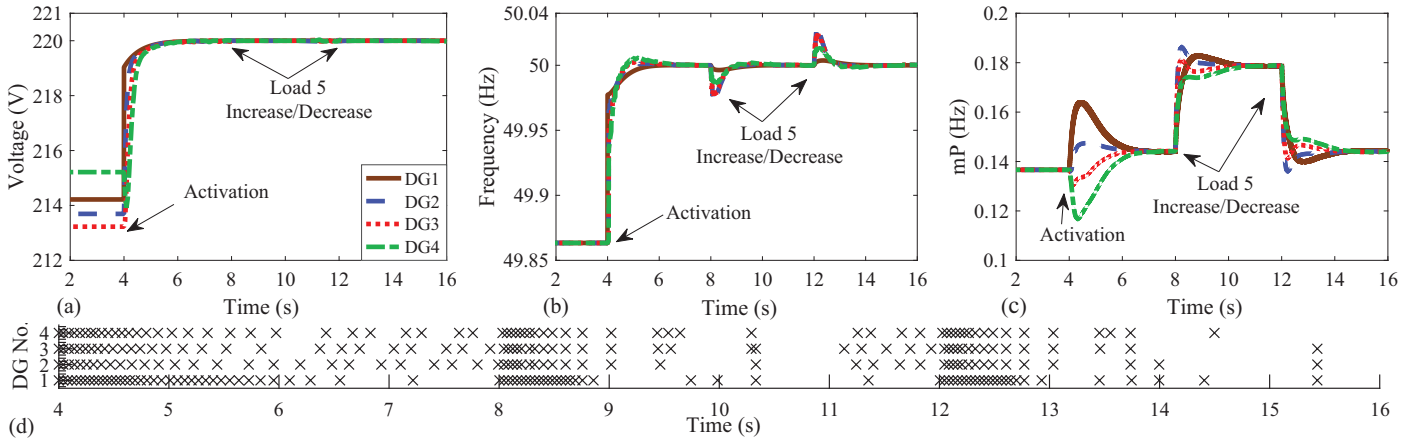

Fig. 3. Performance of the proposed controller; (a) voltages, (b) frequencies, (c) $m_i P_i$s, and (d) communication (triggering) instants.

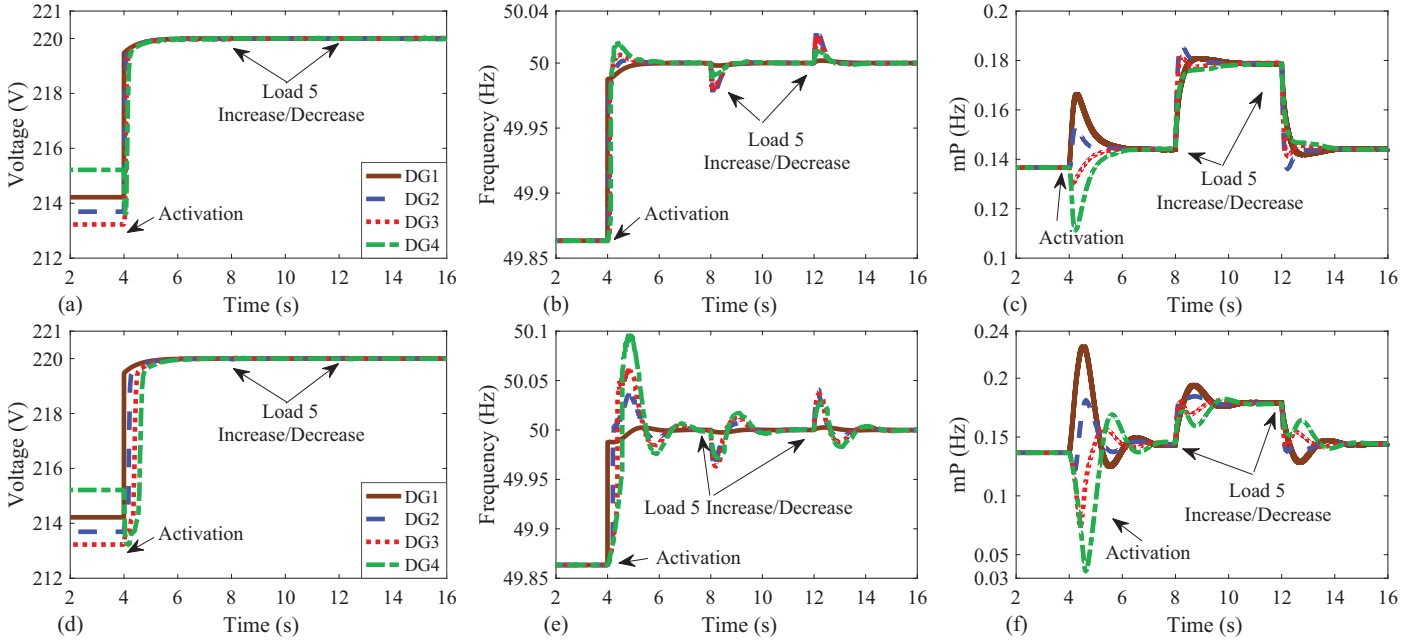

Fig. 4. Performance of the controller with doubled gains under delay of (a)-(c) $0s$ and (d)-(f) $0.16s$; (a)&(d) voltages, (b)&(e) frequencies, and (c)&(f) $m_i P_i$s.

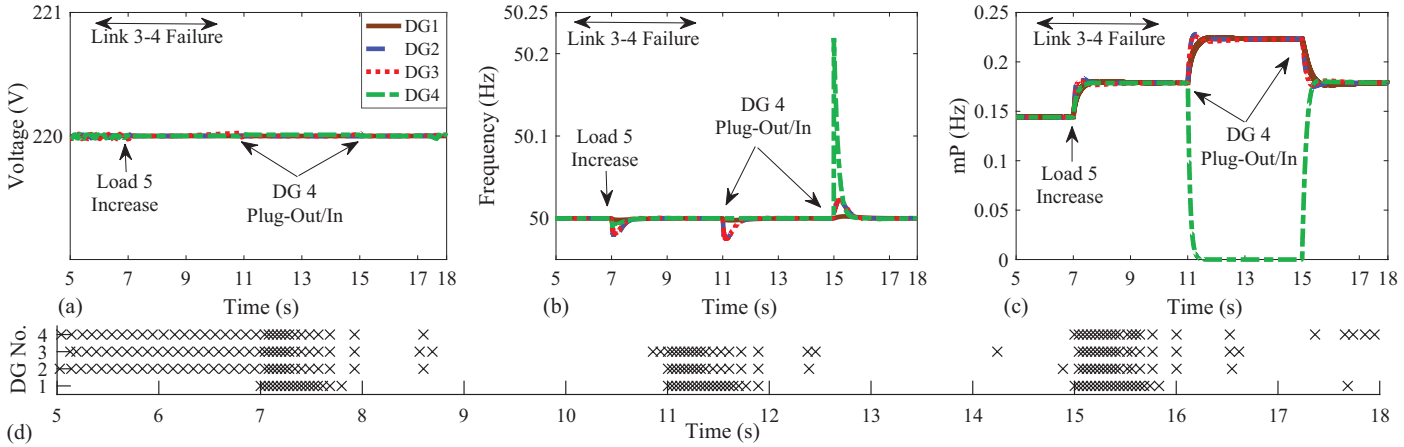

Fig. 5. Link 3-4 failure and plug-and-play capability with 4$^{\text{th}}$ DG; (a) voltages, (b) frequencies, and (c) $m_i P_i$s.

This article has been accepted for publication in a future issue of this journal, but has not been fully edited. Content may change prior to final publication. Citation information: DOI 10.1109/TSG.2019.2945250, IEEE Transactions on Smart Grid

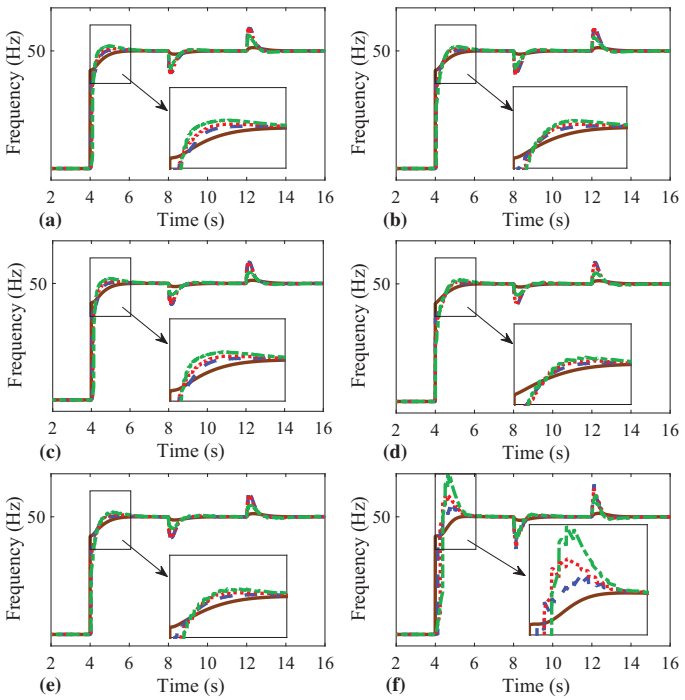

Fig. 6. Impact of different parameters on the frequency responses. **(a)** $\sigma = 0$, $\tau = 1/25$, $\gamma_V, \gamma_\Omega = 0$, **(b)** $\sigma = 0.49$, $\tau = 1/25$, $\gamma_V, \gamma_\Omega = 0$, **(c)** $\sigma = 0$, $\tau = 1/25$, $\gamma_V, \gamma_\Omega \neq 0$, **(d)** $\sigma = 0.49$, $\tau = 0$, $\gamma_V, \gamma_\Omega \neq 0$, **(e)** $\sigma = 0.49$, $\tau = 1/25$, $\gamma_V, \gamma_\Omega \neq 0$, and **(f)** $\sigma = 0.49$, $\tau = 1/8$, $\gamma_V, \gamma_\Omega \neq 0$.

From $t = 6s$ to $t = 10s$ the link between DGs 3 and 4 is interrupted. The circuit breaker CB is intentionally opened at $t = 11s$, and 4$^{\text{th}}$ DG becomes disconnected (its communication links are also interrupted) until $t = 15s$ when the DG joins the secondary controlled MG again. Note that prior to $t = 15s$ a synchronization process is started, CB is closed, and the communication links associated with 4$^{\text{th}}$ DG are all recovered. Fig. 5 depicts the performance of the proposed controller for this scenario. Fig. 5(a)-(c) indicate that *i*) the controller is resilient to the link failure, *ii*) once 4$^{\text{th}}$ DG leaves the MG, other DGs increase their supplied active powers proportional to their ratings and regulate their voltages and frequencies, and *iii*) as soon as 4$^{\text{th}}$ DG connects back to the MG, immediately participates in proportional active power sharing, as well as, voltage and frequency regulation.

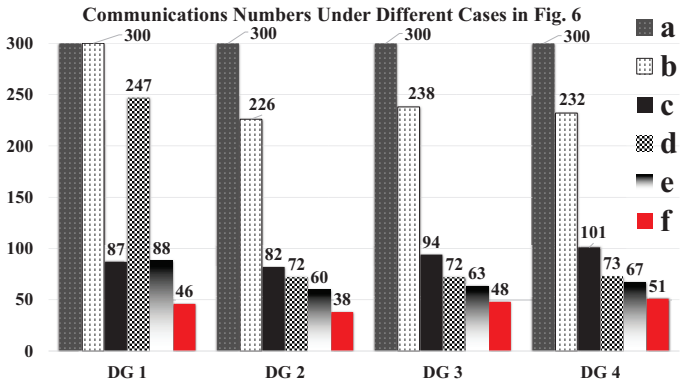

Fig. 7. The number of communications associated with the cases in Fig. 6.

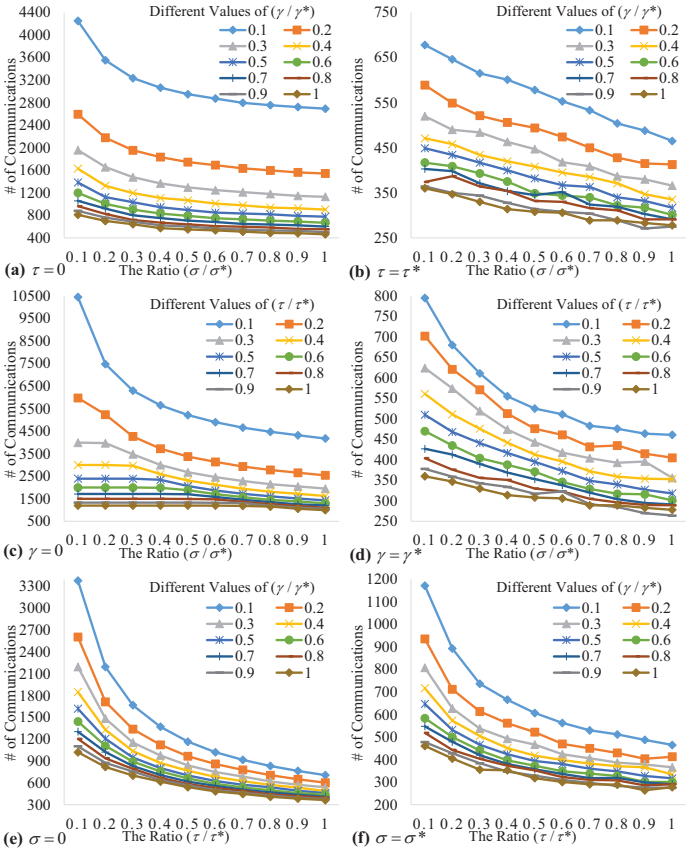

Fig. 8. Parametric graph for total number of communications versus different parameters where $\sigma^* = 0.49$, $\tau^* = 0.04$, $\gamma_\Omega^* = 0.001/2$, and $\gamma_V^* = 0.05/2$.

D. Impacts of Different Parameters

In order to illustrate how different parameters affect the controller performance and the communication burden, the frequency responses and the number of communications for the scenario in Section IV-A ($t \in [4s, 16s]$) are recorded and the results for different cases are given in Fig. 6 and Fig. 7. Note that the cases are defined in the caption of Fig. 6. Comparing the cases (a), (b), (c), and (e) one can see that σ and γ_Ω, γ_V dramatically reduces the communication burden, while some similar satisfactory performances and frequency responses can be achieved; however, γ_Ω and γ_V are more effective than σ. Comparing the cases (d), (e), and (f) one can see that τ reduces the number of communications more effectively while it ensures that the inter-event times are controllable lower-bounded. In addition, from Fig. 6, *i)* the system performance and frequency response under different parameters is reasonable, and *ii*) τ affects the system response similar to a communication delay, inducing transient overshoot and oscillations. To further investigate the parameters' impacts on the communications, the scenario in Section IV-A is re-simulated 600 times for different parameters, and the DGs' total number of communications is figured in Fig. 8. Note that *i)* the parameters are varied with steps of 0.1 of the star-signed values in Fig. 8's caption, and *ii)* the parameters γ_Ω, γ_V are changed together and are simply represented by γ. Generally speaking, all the parameters

TABLE I
COMPARISON OF THIS PAPER WITH PREVIOUS WORKS

Ref.	ET Condition Thresholds			Control Settings	
	State-Dependent	Constant	Time-Dependent	PI-Based	Frequency Consensus
[26]	✓	×	×	×	✓
[27]	✓	✓	×	×	×
[28]	✓	✓	×	×	×
This Paper	✓	✓	✓	✓	×

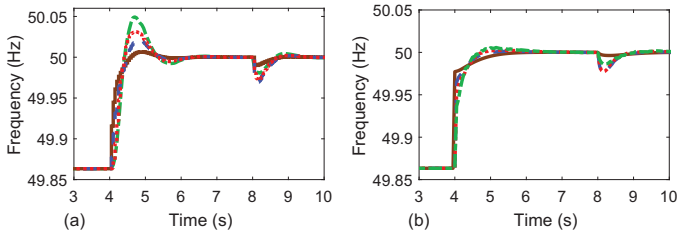

Fig. 9. Freuency responses under (a) the integrator-based frequency-consnesus controller, and (b) the PI-based frequency-consensus-less controller in this paper.

contribute to communication reduction, however, there are some interesting impacts that should be pointed out. According to Fig. 8(a)-(b), increase of γ_Ω and γ_V alleviates the impact of σ on the communication frequency which validates the analyses in the second part of Appendix A-E. Similarly, the increase of τ alleviates the impact of σ. Because, according to the first part of Appendix A-E, in the presence of larger τ the measurement errors grow more, such that after τ seconds they violate the thresholds in (8) more likely; hence, for small values of σ and large values of τ the communications are governed by τ, predominantly. Under periodic time-triggered communications, the number of communications is proportional to the frequency $\frac{1}{\tau}$. However, by incorporating γ_Ω and γ_V into the triggering condition, the communications become *aperiodic* and behave different from the function $\frac{1}{\tau}$. This issue is shown in Fig. 8(e)-(f), where the $\frac{1}{\tau}$ behavior is alleviated as $\frac{\gamma}{\gamma^*}$ increases.

E. Comparison with the Existing Methods

In Table I, the proposed methodology in this paper is compared with the ET controllers in [26]–[28] in terms of triggering conditions and control settings. The controller in this paper compared to those in [26]–[28] is PI-based; in addition, it does not employ frequency leader-following consensus which seems to be redundant in power systems where the frequency reaches agreement per se. Therefore, different from [26] (and also the works in [3]–[11]) and similar to [27], [28], only *one* data does flow between the DGs in frequency-active power control task. Moreover, the employed thresholds in ET condition (7) have state-dependent, constant, and time-dependent parts *at the same time*, resulting in *i)* less communications in both transient and steady-state stages, and *ii)* controllable desired lower bound for inter-event times.

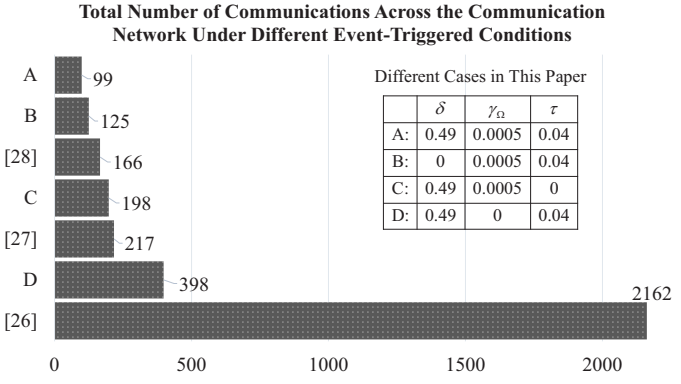

Fig. 10. Comparison between different ET conditions in terms of communication burden across the communication network over $t \in [8s, 16s]$.

In order to highlight the superior performance of the PI-based frequency-consensus-free controller, the frequency response associated with the scenario in Section IV-A (activation and first load change) under the proposed controller is compared with that under the integrator-based leader-following-based controllers. Fig. 9, indicates that the proposed controller demonstrates better transient response.

On the other hand, to compare the mentioned works in terms of communication burden and *ET conditions efficiency*, the case study in Section IV-A is re-simulated for each one, and the total number of all the DGs' communications over $t \in [8s, 16s]$ is figured in Fig. 10. It should be noted that to make a fair comparison it is assumed that *i)* all the DGs can access the frequency reference directly, i.e., $b_i^f = 1, \forall i$, *ii)* since some references do not consider voltage control, the DGs voltages are engaged with the $V-Q$ droop control, i.e., $\Gamma_i = 0, \forall i$, and *iii)* an undirected ring-structured version of the CN in Fig. 2 is established among the DGs, i.e., $b_i^\Omega = 1, a_{ij} = a_{ji}, \forall i, j$. From Fig. 10, one can see how the proposed ET condition with all the state-dpendent, constant, and time-dependent parts, i.e., case A, needs effectively lower data exchange than those needed by the other methods and cases. Moreover, according to the results of the cases A and B, one can see that the success of the proposed triggering instant in reducing the communication burden, owes to the use of τ and γ. It is also shown that even without the constant part, i.e., case D, the proposed condition is more effective than the one in [26]. The reason is that unlike the proposed condition in (7)-(8), the condition in [26] is checked continuously, resulting in a huge number of communications. Under the case C, the ET condition is also checked continuously; however, similar to [27], [28] the condition has a constant part threshold and hence the results in this case are settled in between the results of [27], [28].

V. CONCLUSION

In this paper, the amount of inter-DG communications in secondary control of ac MGs, is highly reduced. Herein, some proportional-integral-based correction terms are introduced wich utilizes an ET data exchange strategy. In this method, some triggering conditions, reducing the communications in both transient and steady-state stages, are employed for directed CNs which ensures that the inter-event time intervals are controllable, lower bounded. Stability and mathematical analyses are also provided. PnP capability of the DGs and the effects of design parameters are clarified, by mathematical analysis and

simulation results. In addition, the results are compared with those of the conventional methods.

APPENDIX A
MATHEMATICAL ANALYSES

Lemma: Let $\mathcal{L}$ be a graph's Laplacian matrix $d_i \geq d_i^o$, one then has $\mathcal{L}\mathbf{1}_n = \mathbf{0}_n$ and $\mathbf{x}^T\mathcal{L}\mathbf{x} \geq \frac{1}{2}\sum_i\sum_{j\in N_i} a_{ij}(x_i - x_j)^2$, where $\mathbf{x} = [x_1, \cdots, x_n]^T \in \mathbb{R}^n$.

Proof of lemma: According to the definition of Laplacian matrix (i.e., $d_i = \sum_{j\in N_i} a_{ij}$), $\mathcal{L}$ has a zero eigenvalue, with $\mathbf{1}_n$ being its corresponding right eigenvector; hence, $\mathcal{L}\mathbf{1}_n = \mathbf{0}_n$. Moreover, one can expand $\mathbf{x}^T\mathcal{L}\mathbf{x}$ and its transpose $\mathbf{x}^T\mathcal{L}^T\mathbf{x}$ as

$$\mathbf{x}^T\mathcal{L}\mathbf{x} = \sum\nolimits_i (d_i x_i^2 - \sum\nolimits_{j\in N_i} a_{ij}x_i x_j),$$
$$\mathbf{x}^T\mathcal{L}^T\mathbf{x} = \sum\nolimits_i (d_i x_i^2 - \sum\nolimits_{j\in N_i} a_{ji}x_i x_j).$$

Now, considering $r_i = d_i - d_i^o$, $d_i = \sum_{j\in N_i} a_{ij}$, and $d_i^o = \sum_{j\in N_i} a_{ji}$, one can rewrite the above equations as

$$\mathbf{x}^T\mathcal{L}\mathbf{x} = \sum\nolimits_i\sum\nolimits_{j\in N_i} (a_{ij}x_i^2 - a_{ij}x_i x_j),$$
$$\mathbf{x}^T\mathcal{L}^T\mathbf{x} = \sum\nolimits_i\sum\nolimits_{j\in N_i} (a_{ij}x_j^2 - a_{ij}x_i x_j) + \sum\nolimits_i r_i x_i^2.$$

Therefore, since $\mathbf{x}^T\mathcal{L}\mathbf{x} = \frac{1}{2}(\mathbf{x}^T\mathcal{L}\mathbf{x} + \mathbf{x}^T\mathcal{L}^T\mathbf{x})$, one can write

$$\mathbf{x}^T\mathcal{L}\mathbf{x} = \frac{1}{2}\sum\nolimits_i\sum\nolimits_{j\in N_i} a_{ij}(x_i - x_j)^2 + \frac{1}{2}\sum\nolimits_i r_i x_i^2.$$

Hence, if $r_i \geq 0$, then $\mathbf{x}^T\mathcal{L}\mathbf{x} \geq \frac{1}{2}\sum_i\sum_{j\in N_i} a_{ij}(x_i - x_j)^2$. ■

A. Secondary Controlled Microgrid System Model

Let $\mathbf{V} = \text{col}\{V_i\}$, $\tilde{\mathbf{V}} = \text{col}\{\tilde{V}_i\}$, $\boldsymbol{\delta} = \text{col}\{\delta_i\}$, $\boldsymbol{\Omega} = \text{col}\{\Omega_i\}$, $\tilde{\boldsymbol{\Omega}} = \text{col}\{\tilde{\Omega}_i\}$, $\hat{\mathbf{P}} = \text{col}\{\hat{P}_i\}$, and $\mathbf{P} = \text{col}\{P_i\}$ be the state column vectors. One can then write (1), (4), and (5) as

$$\begin{aligned}\mathbf{V} &= \mathbf{K}_V\Big(\mathbf{b}_V(V_{ref}\mathbf{1}_n - \mathbf{V}) - (\mathcal{I}_n - \mathbf{b}_V)\mathcal{D}^{-1}\mathcal{L}\tilde{\mathbf{V}}\Big)\\ &+ \mathbf{I}_V\int\Big(\mathbf{b}_V(V_{ref}\mathbf{1}_n - \mathbf{V}) - (\mathcal{I}_n - \mathbf{b}_V)\mathcal{D}^{-1}\mathcal{L}\tilde{\mathbf{V}}\Big)dt,\\ &+ \mathbf{n}\int\dot{\mathbf{Q}}dt - \mathbf{n}\mathbf{Q} + V_{nom}\mathbf{1}_n, \qquad (9a)\\ \boldsymbol{\Omega} &= \mathbf{K}_f\Big(\mathbf{b}_f(\Delta f^*\mathbf{1}_n + \mathbf{m}\mathbf{P} - \boldsymbol{\Omega}) - \mathbf{b}_\Omega\mathcal{D}^{-1}\mathcal{L}\tilde{\boldsymbol{\Omega}}\Big)\\ &+ \mathbf{I}_f\int\Big(\mathbf{b}_f(\Delta f^*\mathbf{1}_n + \mathbf{m}\mathbf{P} - \boldsymbol{\Omega}) - \mathbf{b}_\Omega\mathcal{D}^{-1}\mathcal{L}\tilde{\boldsymbol{\Omega}}\Big)dt, \qquad (9b)\\ \dot{\mathbf{P}} &= -2\pi f_c\mathbf{P} + 2\pi f_c\hat{\mathbf{P}}, \qquad (9c)\\ \dot{\boldsymbol{\delta}} &= 2\pi f_{nom}\mathbf{1}_n + 2\pi\boldsymbol{\Omega} - 2\pi\mathbf{m}\mathbf{P}, \qquad (9d)\end{aligned}$$

where, $\mathbf{K}_V = \text{diag}\{K_i^V\}$, $\mathbf{K}_f = \text{diag}\{K_i^f\}$, $\mathbf{I}_V = \text{diag}\{I_i^V\}$, $\mathbf{I}_f = \text{diag}\{I_i^f\}$, $\mathbf{b}_V = \text{diag}\{b_i^V\}$, $\mathbf{b}_f = \text{diag}\{b_i^f\}$, $\mathbf{b}_\Omega = \text{diag}\{b_i^\Omega\}$ are diagonal matrices; $\Delta f^* = f_{ref} - f_{nom}$. From (2a), $\hat{\mathbf{P}} = \hat{\mathbf{P}}(\mathbf{V}, \boldsymbol{\delta})$ is a function of $\mathbf{V}$, $\boldsymbol{\delta}$ with a Taylor expansion around $\mathbf{x}_b = (V_{ref}\mathbf{1}_n, \mathbf{0}_n)$ as

$$\hat{\mathbf{P}} = \mathbf{G}\mathbf{V} + \mathbf{L}\boldsymbol{\delta} - \hat{\mathbf{P}}(\mathbf{x}_b) + \hat{\mathbf{P}}_{h.o.t}, \qquad (10)$$

where, $\hat{\mathbf{P}}_{h.o.t}$ stands for high-order terms; $\mathbf{L}$ denotes an electrical Laplacian matrix with the adjacency matrix $[V_{ref}^2 B_{ij}]$; $\mathbf{G}$ is a conductance matrix with $V_{ref}(2G_i + \sum_j G_{ij})$ and $V_{ref}G_{ij}$ being its diagonal and off-diagonal entries, respectively. ■

Remark 4: According to the proposed triggering instant (7) described in Algorithm 1, after every triggering instant each DG postpones checking (8a) and (8b) for τ seconds which can be regarded as a sampling-induced time delay. Therefore, in addition to the impacts of the conditions in (8) over the interval $[t_{k_i}^i + \tau, t_{k_i+1}^i)$, the effects of this sampling delay should be investigated. Next, each case is discussed separately.

B. Event-Triggering Conditions Analysis

Considering $\mathbf{e}_V = \tilde{\mathbf{V}} - \mathbf{V}$ and $\mathbf{e}_\Omega = \tilde{\boldsymbol{\Omega}} - \boldsymbol{\Omega}$ and substituting (10) into (9), one can write the system state model as

$$\dot{\mathbf{x}} = \mathbf{A}\mathbf{x} + \mathbf{u}, \text{ where, } \mathbf{u} = \mathbf{C}\mathbf{e} + \mathbf{w}, \qquad (11)$$
$$\text{and, } \mathbf{e} = \begin{bmatrix}\mathbf{e}_V\\ \mathbf{e}_\Omega\end{bmatrix}, \begin{cases}\mathbf{x} = [\mathbf{V}^T\ \boldsymbol{\delta}^T\ \boldsymbol{\Omega}^T\ \mathbf{P}^T]^T,\\ \mathbf{w} = [\mathbf{w}_V^T\ \mathbf{w}_\delta^T\ \mathbf{w}_\Omega^T\ \mathbf{w}_P^T]^T,\end{cases}$$
$$\mathbf{A} = \begin{bmatrix}\mathbf{A}_V & \mathbf{0}_n & \mathbf{0}_n & \mathbf{0}_n\\ \mathbf{0}_n & \mathbf{0}_n & \mathbf{A}_{\delta\Omega} & \mathbf{A}_{\delta P}\\ \mathbf{A}_{\Omega V} & \mathbf{A}_{\Omega\delta} & \mathbf{A}_\Omega & \mathbf{A}_{\Omega P}\\ \mathbf{A}_{PV} & \mathbf{A}_{P\delta} & \mathbf{0}_n & \mathbf{A}_P\end{bmatrix}, \mathbf{C} = \begin{bmatrix}\mathbf{C}_V & \mathbf{0}_n\\ \mathbf{0}_n & \mathbf{0}_n\\ \mathbf{0}_n & \mathbf{C}_\Omega\\ \mathbf{0}_n & \mathbf{0}_n\end{bmatrix};$$

$$\begin{aligned}&\mathbf{M}_V = \mathcal{I}_n + \mathbf{K}_V\mathbf{b}_V + \mathbf{K}_V(\mathcal{I}_n - \mathbf{b}_V)\mathcal{D}^{-1}\mathcal{L}\\ &\mathbf{M}_\Omega = \mathcal{I}_n + \mathbf{K}_f\mathbf{b}_f + \mathbf{K}_f\mathbf{b}_\Omega\mathcal{D}^{-1}\mathcal{L}\\ &\mathbf{A}_V = -\mathbf{M}_V^{-1}\mathbf{I}_V(\mathbf{b}_V + (\mathcal{I}_n - \mathbf{b}_V)\mathcal{D}^{-1}\mathcal{L}),\\ &\mathbf{A}_\Omega = -\mathbf{M}_\Omega^{-1}\mathbf{I}_f(\mathbf{b}_f + \mathbf{b}_\Omega\mathcal{D}^{-1}\mathcal{L}),\ \mathbf{A}_P = -2\pi f_c\mathcal{I}_n,\\ &\mathbf{A}_{\Omega\delta} = 2\pi f_c\mathbf{M}_\Omega^{-1}\mathbf{K}_f\mathbf{b}_f\mathbf{m}\mathbf{L},\ \mathbf{A}_{P\delta} = 2\pi f_c\mathbf{L},\ \mathbf{A}_{\delta\Omega} = 2\pi\mathcal{I}_n,\\ &\mathbf{A}_{\Omega V} = 2\pi f_c\mathbf{M}_\Omega^{-1}\mathbf{K}_f\mathbf{b}_f\mathbf{m}\mathbf{G},\ \mathbf{A}_{PV} = 2\pi f_c\mathbf{G},\\ &\mathbf{A}_{\Omega P} = -\mathbf{M}_\Omega^{-1}(2\pi f_c\mathbf{K}_f\mathbf{b}_f - \mathbf{I}_f\mathbf{b}_f)\mathbf{m},\ \mathbf{A}_{\delta P} = -2\pi\mathbf{m},\\ &\mathbf{C}_V = \mathbf{M}_V^{-1}\mathbf{I}_V(\mathbf{b}_V - \mathcal{I}_n)\mathcal{D}^{-1}\mathcal{L},\ \mathbf{C}_\Omega = -\mathbf{M}_\Omega^{-1}\mathbf{I}_f\mathbf{b}_\Omega\mathcal{D}^{-1}\mathcal{L},\\ &\mathbf{w}_V = \mathbf{M}_V^{-1}(V_{ref}\mathbf{I}_V\mathbf{b}_V\mathbf{1}_n - \mathbf{K}_V(\mathcal{I}_n - \mathbf{b}_V)\mathcal{D}^{-1}\mathcal{L}\dot{\mathbf{e}}_V),\\ &\mathbf{w}_\Omega = \mathbf{M}_\Omega^{-1}(\Delta f^*\mathbf{I}_f\mathbf{b}_f\mathbf{1}_n + \mathbf{K}_f\mathbf{b}_f\mathbf{m}\mathbf{w}_P - \mathbf{K}_f\mathbf{b}_\Omega\mathcal{D}^{-1}\mathcal{L}\dot{\mathbf{e}}_\Omega),\\ &\mathbf{w}_P = 2\pi f_c(\hat{\mathbf{P}}_{h.o.t} - \hat{\mathbf{P}}(\mathbf{x}_b)),\ \mathbf{w}_\delta = 2\pi f_{nom}\mathbf{1}_n, \qquad (12)\end{aligned}$$

Note that $\mathbf{A}$, $\mathbf{x}$, and $\mathbf{w}$ respectively are the state matrix, state vector, and disturbance vector with the components in (12).

Under the conditions in (8) one always has $|e_i^V| < \sigma|\tilde{z}_i^V| + \gamma_V$ and $|e_i^\Omega| < \sigma|\tilde{z}_i^\Omega| + \gamma_\Omega$; therefore

$$|\mathbf{e}_V| \leq \sigma|\mathcal{D}^{-1}\mathcal{L}(\mathbf{V} + \mathbf{e}_V)| + \gamma_V\mathbf{1}_n, \qquad (13a)$$
$$|\mathbf{e}_\Omega| \leq \sigma|\mathcal{D}^{-1}\mathcal{L}(\boldsymbol{\Omega} + \mathbf{e}_\Omega)| + \gamma_\Omega\mathbf{1}_n, \qquad (13b)$$

where, $|\cdot|$ denotes the entry-wise absolute value matrix/vector i.e., $|\mathfrak{M}| = [|\mathfrak{m}_{ij}|], \forall\mathfrak{M} = [\mathfrak{m}_{ij}]$. By using the widely-known triangle inequality one can bound (13) as

$$|\mathbf{e}_V| \leq \sigma|\mathcal{D}^{-1}\mathcal{L}||\mathbf{V}| + \sigma|\mathcal{D}^{-1}\mathcal{L}||\mathbf{e}_V| + \gamma_V\mathbf{1}_n. \qquad (14a)$$
$$|\mathbf{e}_\Omega| \leq \sigma|\mathcal{D}^{-1}\mathcal{L}||\boldsymbol{\Omega}| + \sigma|\mathcal{D}^{-1}\mathcal{L}||\mathbf{e}_\Omega| + \gamma_\Omega\mathbf{1}_n, \qquad (14b)$$

Consider the matrix $\mathcal{M} = \mathbf{I}_n - \sigma|\mathcal{D}^{-1}\mathcal{L}|$. Since $\mathcal{L} = \mathcal{D} - \mathcal{A}$, one has $|\mathcal{D}^{-1}\mathcal{L}| = \mathbf{I}_n + \mathcal{D}^{-1}\mathcal{A}$; thus $\mathcal{M} = (1-\sigma)\mathbf{I}_n - \sigma\mathcal{D}^{-1}\mathcal{A}$. From the Geršgorian discs theorem [34], if $\sigma < 0.5$, all of the eigenvalues of $\mathcal{M}$ have positive real parts. Therefore, according to [35, Th. 5.1.4], $\mathcal{M}$ is *invertible* and (14) can be written as

$$|\mathbf{e}| \leq \mathbf{C}_1|\mathbf{x}| + \mathbf{C}_2, \text{ where, } \mathbf{C}_2 = \begin{bmatrix}\gamma_V\mathcal{M}^{-1}\mathbf{1}_n\\ \gamma_\Omega\mathcal{M}^{-1}\mathbf{1}_n\end{bmatrix},$$
$$\mathbf{C}_1 = \begin{bmatrix}\sigma\mathcal{M}^{-1}|\mathcal{D}^{-1}\mathcal{L}| & \mathbf{0}_n & \mathbf{0}_n & \mathbf{0}_n\\ \mathbf{0}_n & \mathbf{0}_n & \sigma\mathcal{M}^{-1}|\mathcal{D}^{-1}\mathcal{L}|\mathbf{0}_n & \end{bmatrix} \qquad (15)$$

From (11), (15), and the triangle inequality, if $|\mathbf{w}| < w^*\mathbf{1}_{4n}$, then with $\mathcal{T}_1 = |\mathbf{C}|\mathbf{C}_1$ and $\mathcal{T}_2 = |\mathbf{C}|\mathbf{C}_2 + w^*\mathbf{1}_{4n}$ one has

$$|\mathbf{u}| \leq \mathcal{T}_1|\mathbf{x}| + \mathcal{T}_2. \tag{16}$$

The statements (11) and (16)) resemble [36, eq. (28)] and [36, eq. (29)], respectively. Accordingly, if $\mathbf{A}$ in (11) is Hurwitz, the stability and boundedness analyses of the system follows the results of [36, Th. 2]. In other words, the solutions of the system (11) are ultimately uniformly bounded (UUB). The interested reader can refer to [36] for more info on the notion of UUB-ness and the systematic approach for calculating the solutions bounds. According to the foregoing analysis, the system is stable if $\sigma < 0.5$, the matrix $\mathbf{A}$ is Hurwitz, and $|\mathbf{w}| < w^*\mathbf{1}_{4n}$. ■

C. Sampling Delay Effects Analysis

In this part, the focus is on the cybernetic aspect of the system and the underlying physical and control layers i.e., (9b) and (10) are neglected. According to Remark 4, if *over the τ seconds after triggering instants* the measurement errors do not violate the thresholds, the system is the ET control system investigated previously. Otherwise, the time-dependent threshold in (7) introduces a delay of τ to the system and hence one can write $\tilde{\mathbf{V}} = \tilde{\mathbf{V}}(t) = \mathbf{V}(t-\tau)$ & $\tilde{\mathbf{\Omega}} = \tilde{\mathbf{\Omega}}(t) = \mathbf{\Omega}(t-\tau)$. By replacing them in (9) and taking Laplace transform–where s stands for the Laplace operator–one has

$$(s\mathbf{M}' - \mathbf{A}')\mathbf{y} = \mathbf{y}_0 + \frac{1}{s}\mathbf{y}^* + \mathbf{D}'\hat{\mathbf{P}}(s), \text{ where,} \tag{17}$$

$$\mathbf{M}' = \begin{bmatrix} \mathbf{M}'_V & \mathbf{0}_n & \mathbf{0}_n \\ \mathbf{0}_n & \mathbf{M}'_\Omega & \mathbf{0}_n \\ \mathbf{0}_n & \mathbf{0}_n & \mathcal{I}_n \end{bmatrix}, \mathbf{A}' = \begin{bmatrix} \mathbf{A}'_V & \mathbf{0}_n & \mathbf{0}_n \\ \mathbf{0}_n & \mathbf{A}'_\Omega & \mathbf{A}'_{\Omega P} \\ \mathbf{0}_n & \mathbf{0}_n & \mathbf{A}'_P \end{bmatrix},$$

$$\mathbf{y} = \begin{bmatrix} \mathbf{V}(s) \\ \mathbf{\Omega}(s) \\ \mathbf{P}(s) \end{bmatrix}, \mathbf{y}^* = \begin{bmatrix} V_{ref}\mathbf{I}_V\mathbf{b}_V\mathbf{1}_n \\ \Delta f^*\mathbf{I}_f\mathbf{b}_f\mathbf{1}_n \\ \mathbf{0}_n \end{bmatrix}, \mathbf{D}' = \begin{bmatrix} \mathbf{0}_n \\ \mathbf{D}'_\Omega \\ \mathbf{D}'_P \end{bmatrix},$$

$$\mathbf{y}_0 = \begin{bmatrix} (\mathcal{I}_n + \mathbf{K}_V\mathbf{b}_V)\mathbf{V}_0 + \mathbf{K}_V(\mathcal{I}_n - \mathbf{b}_V)\mathcal{D}^{-1}\mathcal{L}\tilde{\mathbf{V}}_0 \\ (\mathcal{I}_n + \mathbf{K}_f\mathbf{b}_f)\mathbf{\Omega}_0 + \mathbf{K}_f\mathbf{b}_\Omega\mathcal{D}^{-1}\mathcal{L}\tilde{\mathbf{\Omega}}_0 \\ \mathbf{P}_0 \end{bmatrix};$$

$$\begin{cases} \mathbf{M}'_V = \mathcal{I}_n + \mathbf{K}_V\mathbf{b}_V + \mathbf{K}_V(\mathcal{I}_n - \mathbf{b}_V)\mathcal{D}^{-1}\mathcal{L}e^{-\tau s}, \\ \mathbf{M}'_\Omega = \mathcal{I}_n + \mathbf{K}_f\mathbf{b}_f + \mathbf{K}_f\mathbf{b}_\Omega\mathcal{D}^{-1}\mathcal{L}e^{-\tau s}, \\ \mathbf{A}'_V = -\mathbf{I}_V\mathbf{b}_V - \mathbf{I}_V(\mathcal{I}_n - \mathbf{b}_V)\mathcal{D}^{-1}\mathcal{L}e^{-\tau s}, \\ \mathbf{A}'_\Omega = -\mathbf{I}_f\mathbf{b}_f - \mathbf{I}_f\mathbf{b}_\Omega\mathcal{D}^{-1}\mathcal{L}e^{-\tau s}, \\ \mathbf{A}'_{\Omega P} = -(2\pi f_c\mathbf{K}_f\mathbf{b}_f - \mathbf{I}_f\mathbf{b}_f)\mathbf{m},\ \mathbf{A}'_P = -2\pi f_c\mathcal{I}_n, \\ \mathbf{D}'_\Omega = 2\pi f_c\mathbf{K}_f\mathbf{b}_f\mathbf{m},\ \mathbf{D}'_P = 2\pi f_c\mathcal{I}_n. \end{cases} \tag{18}$$

Note that $\mathbf{y}$ is the vector of states' Laplace transforms; the zero-sub-scripted quantities in $\mathbf{y}_0$ are initial values' vectors; $\hat{\mathbf{P}}(s)$ is the Laplace transform of the non-filtered power vector $\hat{\mathbf{P}}$.

Let us derive sufficient conditions for stability of the system (17) with the characteristic polynomial $\det(s\mathbf{M}' - \mathbf{A}') = 0$. Since $\mathbf{A}'$, $\mathbf{M}'$ are partitioned triangle matrices, one can write $\det(s\mathbf{M}' - \mathbf{A}') = \det(s\mathbf{M}'_V - \mathbf{A}'_V)\det(s\mathbf{M}'_\Omega - \mathbf{A}'_\Omega)\det(s\mathcal{I}_n - \mathbf{A}'_P)$ and therefore it suffices to analyze the roots of the polynomials $\det(s\mathbf{M}'_V - \mathbf{A}'_V) = 0$, $\det(s\mathbf{M}'_\Omega - \mathbf{A}'_\Omega) = 0$, $\det(s\mathcal{I}_n - \mathbf{A}'_P) = 0$. As the above determinants are zero, the matrices $s\mathbf{M}'_V - \mathbf{A}'_V$, $s\mathbf{M}'_\Omega - \mathbf{A}'_\Omega$, $s\mathcal{I}_n - \mathbf{A}'_P$ are singular; hence, the preceding polynomials have solution *if and only if* one has $x^T(s\mathbf{M}'_V - \mathbf{A}'_V)x = 0$, $x^T(s\mathbf{M}'_\Omega - \mathbf{A}'_\Omega)x = 0$, and $x^T(s\mathcal{I}_n - \mathbf{A}'_P)x = 0$ for some real unit-norm vector x [13]. These are simply scalar polynomials with coefficients in the form of quadratic functions. Therefore, one can extract sufficient conditions of having their roots with negative real parts which is equivalent to the stability of the system. According to (18), $x^T(s\mathcal{I}_n - \mathbf{A}'_P)x = 0$ have roots with negative real parts and hence the stability of the system is boiled down to checking the location of the roots of $x^T(s\mathbf{M}'_V - \mathbf{A}'_V)x = 0$ and $x^T(s\mathbf{M}'_\Omega - \mathbf{A}'_\Omega)x = 0$ that, from (18), one can check the roots of the polynomials below, instead.

$$a_1^V s + a_0^V + (a_2^V s + a_\tau^V)e^{-\tau s} = 0, \tag{19a}$$

$$a_1^\Omega s + a_0^V + (a_2^\Omega s + a_\tau^\Omega)e^{-\tau s} = 0, \tag{19b}$$

where, $a_\tau^V = x^T\mathbf{I}_V(\mathcal{I}_n - \mathbf{b}_V)\mathcal{D}^{-1}\mathcal{L}x$, $a_\tau^V = x^T\mathbf{I}_f\mathbf{b}_\Omega\mathcal{D}^{-1}\mathcal{L}x$, $a_0^V = x^T\mathbf{I}_V\mathbf{b}_V x$, $a_0^\Omega = x^T\mathbf{I}_f\mathbf{b}_f x$, $a_1^V = x^T(\mathcal{I}_n + \mathbf{K}_V\mathbf{b}_V)x$, $a_1^\Omega = x^T(\mathcal{I}_n + \mathbf{K}_f\mathbf{b}_f)x$, $a_2^V = x^T\mathbf{K}_V(\mathcal{I}_n - \mathbf{b}_V)\mathcal{D}^{-1}\mathcal{L}x$, and $a_2^\Omega = x^T\mathbf{K}_f\mathbf{b}_\Omega\mathcal{D}^{-1}\mathcal{L}x$. Equations (19a) and (19b) correspond to [37, Eq. (2.46)]. From the Lemma, if $d_i \geq d_i^o, \forall i$, then a_τ^V, a_τ^Ω, a_2^V, a_2^Ω are positive and hence the system is stable at $\tau = 0$. The roots of (19a) and (19b) are continuous as a function of positive τ. In this way, according to the direct method provided in [37, Chap. 2.3.2], if at some τ roots of (19) cross the imaginary axis, one has $e^{j\omega\tau} = -a_\tau^V/(j\omega e^{j\omega\tau}a_2^V + j\omega a_1^V + a_0^V)$ and $e^{j\omega\tau} = -a_\tau^\Omega/(j\omega e^{j\omega\tau}a_2^\Omega + j\omega a_1^\Omega + a_0^\Omega)$, resulting in (20a) and (20b), respectively (see [37, Eqs. (2.47)-(2.48)]).

$$\begin{cases} \omega^2 = [(a_\tau^V)^2 - (a_0^V)^2]/[(a_1^V)^2 - (a_2^V)^2], \\ \omega\tau = \arg(-\frac{j\omega a_2^V + a_\tau^V}{j\omega a_1^V + a_0^V}) + 2\pi k, k = 0, 1, \cdots, \end{cases} \tag{20a}$$

$$\begin{cases} \omega^2 = [(a_\tau^\Omega)^2 - (a_0^\Omega)^2]/[(a_1^\Omega)^2 - (a_2^\Omega)^2], \\ \omega\tau = \arg(-\frac{j\omega a_2^\Omega + a_\tau^\Omega}{j\omega a_1^\Omega + a_0^\Omega}) + 2\pi k, k = 0, 1, \cdots, \end{cases} \tag{20b}$$

where, $\arg(\cdot)$ denotes the argument operator. From [37, Prop. 2.1], if (19) with $\tau = 0$ is stable and the first lines of (20a) and (20b) do not have solutions, then the polynomials in (19) are delay-independent stable (independent of τ). Otherwise, the first-line equations in (20a) and (20b) yield the positive crossing frequencies $\omega_c^V = \sqrt{(a_\tau^V)^2 - (a_0^V)^2}/\sqrt{(a_1^V)^2 - (a_2^V)^2}$ and $\omega_c^\Omega = \sqrt{(a_\tau^\Omega)^2 - (a_0^\Omega)^2}/\sqrt{(a_1^\Omega)^2 - (a_2^\Omega)^2}$, respectively. Substituting these crossing frequencies for ω in the argument equations in (20a) and (20b), respectively, one can obtain the respective crossing delays as

$$\tau_k^V\omega_c^V = \pi + \arctan(\tfrac{a_2^V\omega_c}{a_\tau^V}) - \arctan(\tfrac{a_1^V\omega_c}{a_0^V}) + 2\pi k, \tag{21a}$$

$$\tau_k^\Omega\omega_c^\Omega = \pi + \arctan(\tfrac{a_2^\Omega\omega_c}{a_\tau^\Omega}) - \arctan(\tfrac{a_1^\Omega\omega_c}{a_0^\Omega}) + 2\pi k, \tag{21b}$$

where, $k = 0, 1, \cdots$. Correspondingly,

$$\tau_0^V = \left(\pi + \arctan(\tfrac{a_2^V\omega_c^V}{a_\tau^V}) - \arctan(\tfrac{a_1^V\omega_c^V}{a_0^V})\right)/\omega_c^V, \tag{22a}$$

$$\tau_0^\Omega = \left(\pi + \arctan(\tfrac{a_2^\Omega\omega_c^\Omega}{a_\tau^\Omega}) - \arctan(\tfrac{a_1^\Omega\omega_c^\Omega}{a_0^\Omega})\right)/\omega_c^\Omega; \tag{22b}$$

which implies the stability for $\tau < \min(\tau_0^V, \tau_0^\Omega)$. ■

D. Equilibrium Analysis

According to (4a), in steady state one has

$$b_i^f(f_{ref} - f_{com}) + \tfrac{b_i^\Omega}{d_i}\sum\nolimits_{j\in N_i} a_{ij}(\tilde{\Omega}_j - \tilde{\Omega}_i) = 0, \tag{23}$$

where, f_{com} is common frequency. Eq. (23) can be written as

$$\mathbf{b}_f(f_{com} - f_{ref})\mathbf{1}_n + \mathbf{b}_\Omega \mathcal{D}^{-1}\mathcal{L}\tilde{\mathbf{\Omega}} = \mathbf{0}_n, \tag{24}$$

corresponding to [14, eq.(8)]. Therefore, if the CN among the DGs has a rooted spanning tree and $b_i \neq 0$ for at least one root node, then the results of [14, Th. 2] hold, i.e., in steady state one has $f_i = f_{ref}$, $\tilde{\Omega}_i = \tilde{\Omega}_j$, $\forall i, j$. One can bound the neighborhood error of Ω_i as

$$|\tfrac{1}{d_i}\sum a_{ij}(\Omega_j - \Omega_i)| \leq |\tilde{z}_i^\Omega| + \tfrac{1}{d_i}\sum a_{ij}(|e_j| + |e_i|). \tag{25}$$

From (1d), (8a), & (25), in steady state when $\tilde{z}_i^\Omega = 0$, one has

$$m_i P_i = \Omega_i \Rightarrow |\tfrac{1}{d_i}\sum a_{ij}(m_j P_j - m_i P_i)| \leq 2\gamma_\Omega. \tag{26}$$

The last inequality implies that in steady state, the active powers are shared properly but with the maximum neighborhood error of $2\gamma_\Omega$ Hertz. According to (1d), this error can be translated into (regarded as) steady-state frequency error.

From (4b), if $b_i^V = 1$, i.e., the DG voltage is not affected by its neighbors, then in steady state one has $V_i = V_{ref}$. Otherwise, its steady-state voltage is influenced by their in-neighbors. Let $z_i^V = \frac{1}{d_i}\sum_j a_{ij}(V_j - V_i), \forall d_i \neq 0$ be the neighborhood voltage error. Then, one has $z_i^V = \tilde{z}_i^V - \frac{1}{d_i}\sum_j a_{ij}(e_j^V - e_i^V)$. From (9a), one has $(b_i^V - 1)\tilde{z}_i^V = b_i^V \Delta V_i$ in steady state. By using these equations, (8b), and the triangle inequality one has

$$|z_i^V| \leq 2\gamma_V, \quad \forall i | b_i^V = 0. \tag{27}$$

Hence, the maximum *neighborhood voltage error* is $2\gamma_V$. ■

E. Inter-Event Time Analysis

Transient effects of τ: Consider the functions $y_i^\Omega = |e_i^\Omega|$ and $y_i^V = |e_i^V|$ over $[t_{k_i}^i, t_{k_i+1}^i)$. According to the event-triggering condition in (7), the inter-event time intervals are always greater than τ. In what follows the growth of the functions y_i^Ω and y_i^V over the first τ seconds after triggering instant $t_{k_i}^i$ is investigated. Differentiating them by using (4) yields $\dot{y}_i^\Omega \leq |\dot{\Omega}_i| \leq \alpha_{k_i}^\Omega$ and $\dot{y}_i^V \leq |\dot{V}_i| \leq \alpha_{k_i}^V$; where, $\alpha_{k_i}^\Omega$ and $\alpha_{k_i}^V$ are the corresponding maximum values over $[t_{k_i}^i, t_{k_i+1}^i)$. Considering $y_i^\Omega(t_{k_i}^i) = y_i^V(t_{k_i}^i) = 0$ and integrating these inequalities, one can write $y_i^\Omega(t_{k_i}^i + \tau) \leq \alpha_{k_i}^\Omega \tau$ and $y_i^V(t_{k_i}^i + \tau) \leq \alpha_{k_i}^V \tau$, which demonstrate the maximum possible growth of measurement errors over the first τ seconds and can be used for proper selection of τ.

Inter-event times: According to (7), if $y_i^\Omega(t_{k_i}^i + \tau) > \sigma b_i^\Omega |\tilde{z}_i^\Omega| + \gamma_\Omega$ or $y_i^V(t_{k_i}^i + \tau) > \sigma(1 - b_i^V)|\tilde{z}_i^V| + \gamma_V$, then $t_{k_i+1}^i - t_{k_i}^i = \tau$, otherwise $t_{k_i+1}^i - t_{k_i}^i > \tau$. For the second case, considering $y_i^\Omega(t_{k_i}^i) = y_i^V(t_{k_i}^i) = 0$ and integrating $\dot{y}_i^\Omega \leq \alpha_{k_i}^\Omega$, $\dot{y}_i^V \leq \alpha_{k_i}^V$ one has $y_i^\Omega \leq \alpha_{k_i}^\Omega(t - t_{k_i}^i)$ and $y_i^V \leq \alpha_{k_i}^V(t - t_{k_i}^i)$. From (8), the next event time $t_{k_i+1}^i$ is when $y_i^\Omega > \sigma b_i^\Omega |\tilde{z}_i^\Omega| + \gamma_\Omega$ or $y_i^V > \sigma(1 - b_i^V)|\tilde{z}_i^V| + \gamma_V$. Hence, if $t_{k_i+1}^i - t_{k_i}^i > \tau$, then

$$t_{k_i+1}^i - t_{k_i}^i > \min(\tau_{k_i}^\Omega, \tau_{k_i}^V) = \tau_{k_i} \tag{28}$$

where $\alpha_{k_i}^\Omega \tau_{k_i}^\Omega = \sigma b_i^\Omega |\tilde{z}_i^\Omega| + \gamma_\Omega$ and $\alpha_{k_i}^V \tau_{k_i}^V = \sigma(1 - b_i^V)|\tilde{z}_i^V| + \gamma_V$. The bound in (28) is a function of $\sigma \in [0, 0.5)$, γ_Ω, and γ_V. Accordingly, if $\gamma_i^\Omega = \gamma_i^V = 0$ then τ_i^Ω and τ_i^V are proportional to σ, i.e., the more σ, the less τ_i^Ω, τ_i^V, and the more communications. In fact, the parameters γ_i^Ω, γ_i^V alleviate the impact of σ on the communication and inter-event time.

All in all, if τ is small then the inter-event times are highly affected by σ, γ_Ω, and γ_V such that the more σ, γ_Ω, and γ_V, the more inter-event times, and the less communications. But then, for large values of τ the inter-event times are mainly affected by τ and the other parameters have less effects. ■

REFERENCES

[1] Y. Han, H. Li, P. Shen, E. A. A. Coelho, and J. M. Guerrero, "Review of active and reactive power sharing strategies in hierarchical controlled microgrids," *IEEE Trans. Power Electron.*, vol. 32, no. 3, pp. 2427–2451, Mar. 2017.

[2] M. Yazdanian and A. Mehrizi-Sani, "Distributed control techniques in microgrids," *IEEE Trans. Smart Grid*, vol. 5, no. 6, pp. 2901–2909, Nov. 2014.

[3] A. Bidram, A. Davoudi, F. L. Lewis, and J. M. Guerrero, "Distributed cooperative secondary control of microgrids using feedback linearization," *IEEE Trans. Power Syst.*, vol. 28, no. 3, pp. 3462–3470, Aug. 2013.

[4] A. Bidram, A. Davoudi, F. L. Lewis, and Z. Qu, "Secondary control of microgrids based on distributed cooperative control of multi-agent systems," *IET Gener. Transm. Distrib.*, vol. 7, no. 8, pp. 822–831, Aug. 2013.

[5] A. Bidram, F. L. Lewis, and A. Davoudi, "Distributed control systems for small-scale power networks: Using multiagent cooperative control theory," *IEEE Control Syst. Mag.*, vol. 34, no. 6, pp. 56–77, Dec. 2014.

[6] N. M. Dehkordi, N. Sadati, and M. Hamzeh, "Fully distributed cooperative secondary frequency and voltage control of islanded microgrids," *IEEE Trans. Energy Convers.*, vol. 32, no. 2, pp. 675–685, Jun. 2017.

[7] F. Guo, C. Wen, J. Mao, and Y. D. Song, "Distributed secondary voltage and frequency restoration control of droop-controlled inverter-based microgrids," *IEEE Trans. Ind. Electron.*, vol. 62, no. 7, pp. 4355–4364, Jul. 2015.

[8] S. Zuo, A. Davoudi, Y. Song, and F. L. Lewis, "Distributed finite-time voltage and frequency restoration in islanded ac microgrids," *IEEE Trans. Ind. Electron.*, vol. 63, no. 10, pp. 5988–5997, Oct. 2016.

[9] N. M. Dehkordi, N. Sadati, and M. Hamzeh, "Distributed robust finite-time secondary voltage and frequency control of islanded microgrids," *IEEE Trans. Power Syst.*, vol. 32, no. 5, pp. 3648–3659, Sept. 2017.

[10] A. Pilloni, A. Pisano, and E. Usai, "Robust finite-time frequency and voltage restoration of inverter-based microgrids via sliding-mode cooperative control," *IEEE Trans. Ind. Electron.*, vol. 65, no. 1, pp. 907–917, Jan. 2018.

[11] N. M. Dehkordi, H. R. Baghaee, N. Sadati, and J. M. Guerrero, "Distributed noise-resilient secondary voltage and frequency control for islanded microgrids," *IEEE Trans. Smart Grid*, vol. 10, no. 4, pp. 3780–3790, Jul. 2019.

[12] L. Y. Lu and C. C. Chu, "Consensus-based droop control synthesis for multiple DICs in isolated micro-grids," *IEEE Trans. Power Syst.*, vol. 30, no. 5, pp. 2243–2256, Sep. 2015.

[13] J. W. Simpson-Porco, Q. Shafiee, F. Dörfler, J. C. Vasquez, J. M. Guerrero, and F. Bullo, "Secondary frequency and voltage control of islanded microgrids via distributed averaging," *IEEE Trans. Ind. Electron.*, vol. 62, no. 11, pp. 7025–7038, Nov. 2015.

[14] B. Abdolmaleki, Q. Shafiee, and H. Bevrani, "Kron reduction and L_2-stability for plug-and-play frequency control of microgrids," in *Proc. 2018 Smart Grid Conference (SGC)*, Sanandaj, Iran, Nov. 2018, pp. 1–6.

[15] Q. Yang, J. A. Barria, and T. C. Green, "Communication infrastructures for distributed control of power distribution networks," *IEEE Trans. Ind. Informat.*, vol. 7, no. 2, pp. 316–327, May 2011.

[16] G. Xie, H. Liu, L. Wang, and Y. Jia, "Consensus in networked multi-agent systems via sampled control: fixed topology case," in *Proc. 2009 American Control Conference*, St. Louis, MO, USA, Jun. 2009, pp. 3902–3907.

[17] L. Ding, Q. L. Han, X. Ge, and X. M. Zhang, "An overview of recent advances in event-triggered consensus of multiagent systems," *IEEE Trans. Cybern.*, vol. 48, no. 4, pp. 1110–1123, Apr. 2018.

[18] X. M. Zhang, Q. L. Han, and B. L. Zhang, "An overview and deep investigation on sampled-data-based event-triggered control and filtering for networked systems," *IEEE Trans. Ind. Informat.*, vol. 13, no. 1, pp. 4–16, Feb. 2017.

[19] M. Tahir and S. K. Mazumder, "Self-triggered communication enabled control of distributed generation in microgrids," *IEEE Trans. Ind. Informat.*, vol. 11, no. 2, pp. 441–449, Apr. 2015.

[20] W. Meng, X. Wang, and S. Liu, "Distributed load sharing of an inverter-based microgrid with reduced communication," *IEEE Trans. Smart Grid*, vol. 9, no. 2, pp. 1354–1364, Mar. 2017.

[21] Y. Fan, G. Hu, and M. Egerstedt, "Distributed reactive power sharing control for microgrids with event-triggered communication," *IEEE Trans. Control Syst. Technol.*, vol. 25, no. 1, pp. 118–128, Jan. 2017.

[22] R. Han, N. L. D. Aldana, L. Meng, J. M. Guerrero, and Q. Sun, "Droop-free distributed control with event-triggered communication in dc microgrid," in *Proc. IEEE Applied Power Electronics Conference and Exposition (APEC)*, Tampa, FL, USA, Mar. 2017, pp. 1160–1166.

[23] R. Han, L. Meng, J. M. Guerrero, and J. C. Vasquez, "Distributed nonlinear control with event-triggered communication to achieve current-sharing and voltage regulation in dc microgrids," *IEEE Trans. Power Electron.*, vol. 33, no. 7, pp. 6416–6433, Jul. 2018.

[24] J. Zhou, H. Zhang, Q. Sun, D. Ma, and B. Huang, "Event-based distributed active power sharing control for interconnected ac and dc microgrids," *IEEE Trans. Smart Grid*, vol. 9, no. 6, pp. 6815–6828, Nov. 2018.

[25] S. Sahoo and S. Mishra, "An adaptive event-triggered communication based distributed secondary control for dc microgrids," *IEEE Trans. Smart Grid*, vol. 9, no. 6, pp. 6674–6683, Nov. 2018.

[26] M. Chen, X. Xiao, and J. M. Guerrero, "Secondary restoration control of islanded microgrids with decentralized event-triggered strategy," *IEEE Trans. Ind. Informat.*, vol. 14, no. 9, pp. 3870–3880, Sep. 2018.

[27] B. Abdolmaleki, Q. Shafiee, M. M. Arefi, and T. Dragičević, "An instantaneous event-triggered Hz-Watt control for microgrids," *IEEE Trans. Power Syst.*, vol. 34, no. 5, pp. 3616–3625, Sep. 2019.

[28] S. Weng, D. Yue, C. Dou, J. Shi, and C. Huang, "Distributed event-triggered cooperative control for frequency and voltage stability and power sharing in isolated inverter-based microgrid," *IEEE Trans. Cybern.*, vol. 49, no. 4, pp. 1427–1439, Apr. 2019.

[29] A. Bidram, F. L. Lewis, and A. Davoudi, "Synchronization of nonlinear heterogeneous cooperative systems using inputoutput feedback linearization," *Automatica*, vol. 50, no. 10, pp. 2578–2585, Oct. 2014.

[30] R. Olfati-Saber, J. A. Fax, and R. M. Murray, "Consensus and cooperation in networked multi-agent systems," *Proc. IEEE*, vol. 95, no. 1, pp. 215–233, Jan. 2007.

[31] A. Yazdani and R. Iravani, *Voltage-Sourced Converters in Power Systems: Modeling, Control, and Applications*. John Wiley & Sons, 2010.

[32] X. Wu, C. Shen, and R. Iravani, "Feasible range and optimal value of the virtual impedance for droop-based control of microgrids," *IEEE Trans. Smart Grid*, vol. 8, no. 3, pp. 1242–1251, May 2017.

[33] J. Schiffer, R. Ortega, A. Astolfi, J. Raisch, and T. Sezi, "Conditions for stability of droop-controlled inverter-based microgrids," *Automatica*, vol. 50, no. 10, pp. 2457–2469, Oct. 2014.

[34] R. A. Horn and C. R. Johnson, *Matrix Analysis*. Cambridge University Press, 2012.

[35] H. Anton and C. Rorres, *Elementary Linear Algebra: Applications Version*, 11st ed. Wiley Global Education, 2013.

[36] E. Kofman, H. Haimovich, and M. M. Seron, "A systematic method to obtain ultimate bounds for perturbed systems," *International Journal of Control*, vol. 80, no. 2, pp. 167–178, Feb. 2007.

[37] E. Fridman, *Introduction to time-delay systems: Analysis and control*. Springer, 2014.

Babak Abdolmaleki (S'17-M'18-19) was born in Kurdistan, Iran, in 1992. He received his B.Sc. and M.Sc. degrees in Electrical Engineering from Shiraz University, Shiraz, Iran, in 2014 and 2017, respectively. Since 2017, he has been with the Smart/Micro Grids Research Center, University of Kurdistan, Sanandaj, Iran, as a Research Associate.

His main research interests are centered around distributed optimization and control, event-triggered control, advanced control of power converters, and modern power systems dynamics and control.

Qobad Shafiee (S'13-M'15-SM'17) received Ph.D. degree in electrical engineering from the Department of Energy Technology, Aalborg University (Denmark) in 2014. He is currently an Assistant Professor, Associate Director of International Relations, and the Program Co-Leader of the Smart/Micro Grids Research Center at the University of Kurdistan, Sanandaj, Iran, where he was a lecturer from 2007 to 2011. In 2014, he was a Visiting Scholar with the Electrical Engineering Department, the University of Texas at Arlington, Arlington, TX, USA. He was a Post-Doctoral Fellow with the Department of Energy Technology, Aalborg University in 2015.

His current research interests include modeling, energy management, control of power electronics-based systems and microgrids, and model predictive and optimal control of modern power systems.

Ali Reza Seifi was born in Shiraz, Iran, in 1968. He received the B.Sc. degree from Shiraz University, Shiraz, Iran, in 1991, the M.Sc. degree from the University of Tabriz, Tabriz, Iran, in 1993, and the Ph.D. degree from Tarbiat Modarres University, Tehran, Iran, in 2001, all in Electrical Engineering. He is currently a Professor with the Department of Power and Control Engineering, School of Electrical and Computer Engineering, Shiraz University. His research interests are power and energy systems, electrical machines, energy management, and fuzzy optimization.

Mohammad Mehdi Arefi (M'17-SM'17) was born in 1982. He received the B.Sc. degree from the Department of Electrical Engineering, Shiraz University, Shiraz, Iran, in 2004, and the M.Sc. and Ph.D. degrees from the Electrical Engineering Department, Iran University of Science and Technology, Tehran, Iran, in 2007 and 2011, respectively. He is an Associate Professor with the Department of Power and Control Engineering, School of Electrical and Computer Engineering, Shiraz University.

His current research interests include adaptive robust control, nonlinear and chaos control, and application of control methods in power systems.

Frede Blaabjerg (S'86-M'88-SM'97-F'03) was with ABB-Scandia, Randers, Denmark, from 1987 to 1988. From 1988 to 1992, he got the Ph.D. degree in Electrical Engineering at Aalborg University in 1995. He became an Assistant Professor in 1992, an Associate Professor in 1996, and a Full Professor of power electronics and drives in 1998. From 2017 he became a Villum Investigator. He is honoris causa at University Politehnica Timisoara (UPT), Romania and Tallinn Technical University (TTU) in Estonia.

His current research interests include power electronics and its applications such as in wind turbines, PV systems, reliability, harmonics and adjustable speed drives. He has published more than 600 journal papers in the fields of power electronics and its applications. He is the co-author of four monographs and editor of ten books in these fields.

He has received 31 IEEE Prize Paper Awards, the IEEE PELS Distinguished Service Award 2009, the EPE-PEMC Council Award 2010, the IEEE William E. Newell Power Electronics Award 2014, the Villum Kann Rasmussen Research Award 2014 and the Global Energy Prize in 2019. He was the Editor-in-Chief of the IEEE TRANSACTIONS ON POWER ELECTRONICS from 2006 to 2012. He has been Distinguished Lecturer for the IEEE Power Electronics Society from 2005 to 2007 and for the IEEE Industry Applications Society from 2010 to 2011 as well as 2017 to 2018. In 2019-2020 he serves as President of IEEE Power Electronics Society. He is Vice-President of the Danish Academy of Technical Sciences too. He is nominated in 2014-2018 by Thomson Reuters to be between the most 250 cited researchers in Engineering in the world.